Available online at www.sciencedirect.com
SCIENCE DIRECT®
Biomaterials 26 (2005) 1381–1388
Biomaterials
www.elsevier.com/locate/biomaterials

Photo-immobilization of a phospholipid polymer for surface modification

Tomohiro Konno[a,b], Hirokazu Hasuda[a], Kazuhiko Ishihara[b], Yoshihiro Ito[a,*]

[a] *Regenerative Medical Bioreactor Project, Kanagawa Academy of Science and Technology, KSP East 309, 3-2-1 Sakado, Takatsu-ku, Kawasaki, Kanagawa 213-0012, Japan*

[b] *Department of Materials Engineering, Graduate School of Engineering, The University of Tokyo, 7-3-1, Hongo, Bunkyo-ku, Tokyo 113-8656, Japan*

Received 27 December 2003; accepted 30 April 2004

Available online 19 June 2004

Abstract

A photo-reactive polymer having a phospholipid polar group was prepared, and the polymer was photo-immobilized on polymeric surfaces, where its interactions with biocomponents were investigated. By using a photo-immobilization method, the polymer was used for surface modification of polyethylene and polypropylene, polymers whose surfaces were not treated in our previous development of the phosphorylcholine-derived polymer. The photo-reactive polymer was synthesized by a coupling reaction involving copolymer consisting of 2-methacryloyloxyethyl phosphorylcholine and methacrylic acid with 4-azidoaniline. When the polymer was unpattern immobilized on the surface, X-ray photo-electron spectroscopic analysis and static contact angle measurements were performed. It was shown that the surface was covered with phospholipid polar groups. Micropattern immobilization was carried out using a micropatterned photo-mask. Measurements using atomic force microscopy showed that the swelled micropatterned polymer was five times as thick as the dried one. Protein adsorption and platelet adhesion were reduced on the polymer-immobilized regions. Mammalian cells did not adhere, and formed aggregates on the immobilized regions. In conclusion, the photo-reactive phospholipid polymer was covalently immobilized on the conventional polymer surfaces and it tended to reduce interactions with proteins and cells.

Keywords: Photo-immobilization; Phospholipid polymer; Surface modification; Protein adsorption; Cell adhesion

1. Introduction

Lipid membranes are used as biomimetic systems, and are expected to become a key component of novel biomolecular materials [1–14]. In particular, lipid bilayer membranes on solid supports have been the subject of numerous publications [1–11]. The membranes prepared on various solids by optimized variations of the available deposition chemistries have been shown to accommodate a variety of proteins and enzymes in controlled orientations and in active conformations. The supported lipid bilayer is considered to mimic the native environment of membrane-associated biomolecules. These membranes are also promising surfaces for developing new biosensors and coating materials that resist non-specific interactions with proteins and cells.

The lipid head group of phosphorylcholine, a zwitterion, is a common group in the lipid molecules that form biological membranes, and is considered to play an important role as a surface material for biomedical devices by reducing interaction with proteins and cells. As a biomimetic polymer, 2-methacryloyloxyethyl phosphorylcholine (MPC)-containing polymer was synthesized by the group of Ishihara and Nakabayashi [15,16]. The polymer shows non-thrombogenicity, that is, suppression of non-specific protein adsorption, platelet adhesion, activation, and aggregation when the polymer contacted whole blood, even in the absence of anticoagulants.

Recently, some types of MPC-containing copolymers have been synthesized for coating [17] and covalent immobilization was achieved [18–20]. However, the

*Corresponding author. Tel.: +81-44-819-2044; fax: +81-44-819-2039.

E-mail address: y-ito@ksp.or.jp (Y. Ito).

0142-9612/$ - see front matter © 2004 Elsevier Ltd. All rights reserved.
doi:10.1016/j.biomaterials.2004.04.047

covalent immobilization was limited to specialized surfaces. Therefore, in the present investigation, photo-immobilization was employed for covalent immobilization of the polymer on a broader variety of surfaces.

In addition, although many synthetic polymers have been devised to improve surface reducing interaction with proteins or cells, it is difficult to directly compare the surface properties of different polymers under precisely the same conditions. Therefore, a micropatterning method has been devised for lipids and polymers [21–23], and the method has proved useful for comparing the interaction of polymers with proteins and cells [24–26]. We modified the method of Matsuda and Sugawara [27], and have applied this method to some growth factors [28–30], sulfated hyaluronic acid [31], heparin [32], and thermo-responsive polymer [33]. In the present study, micropatterning of MPC polymer was performed, and the interactions with proteins and cells were investigated.

2. Materials and methods

2.1. Synthesis of photo-reactive MPC polymer

The polymer synthesis is illustrated in Fig. 1. MPC copolymer consisting of MPC (90 mol%) and methacrylic acid (10 mol%) was obtained from NOF Co. Ltd. (Tokyo, Japan), and is referred to as PMAc. The molecular weight of PMAc, as measured by gel permeation chromatography, was 2.2×10^5. Modification of PMAc was performed as follows: 4-azidoaniline (12.44 mg) and water-soluble carbodiimide (17.47 mg) were dissolved in 2 ml of PMAc solution (5 wt%) and 98 ml of water was added to the solution. The solution was left to stand for 24 h. After the reaction, the product was dialyzed with dialysis cassette (PIERCE, Rockford, IL) until no further release of azidoaniline through the cassette was confirmed by ultraviolet (UV) absorption. The resultant solution was freeze-dried. The azidophenyl-derivatized PMAc is referred to as Az-PMAc. Elemental analysis indicated that the amount of azidophenyl group in Az-PMAc was 6%.

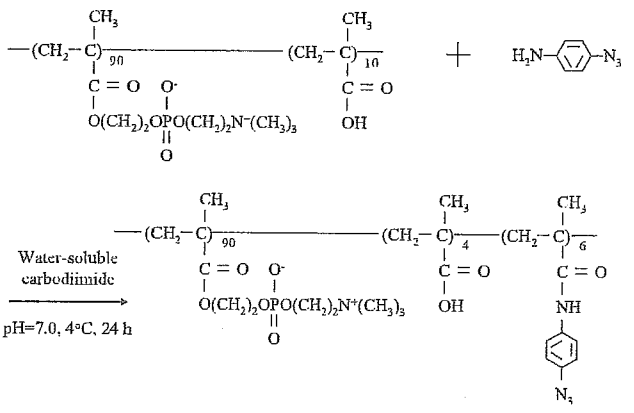

Fig. 1. Synthetic scheme for photo-reactive phosphorylcholine-containing polymer.

2.2. Micropatterning

The micropatterning method is illustrated in Fig. 2. An aqueous solution of Az-PMAc (1 wt%) was cast on polyethylene and polypropylene plates (diameter 22 mm), which were purchased from Sarstedt (Newton, NC) and from Nikkyo Technos Co. Ltd. (Tokyo, Japan), respectively, and air-dried at room temperature. Subsequently, the plate was covered with a photo-mask, which was manufactured by Toppan Printing Co. Ltd. (Tokyo, Japan) and was UV-irradiated with a UV lamp (UV Spot Light Source L5662, Hamamatsu Photonics, Hamamatsu, Japan) from a distance of 5 cm for 10 s ($16\,mW/cm^2$). When an unpatterned surface was prepared, the photo-mask was not employed. The plate was then repeatedly washed with distilled water.

2.3. Measurement of contact angle

The unpatterned sample was placed on the holder of a CA-W Automatic Contact Angle Meter (Kyowa Interface Science Co. Ltd., Saitama, Japan) and a drop of water (0.4 μl) was put on the sample surface. The contact angle of the drop on the surface was measured at room temperature. At least 10 contact angles on different areas were measured and averaged.

2.4. Measurement by X-ray photo-electron spectroscopy (XPS)

The unpatterned sample was inserted in the holder of an XPS, AXIS-HSi (Shimadzu/Kratos, Kyoto, Japan). After evacuation, the measurement was carried out under 3×10^{-9} Torr. The X-ray source was CuK_α, the applied voltage was 12 kV, and the electric current was

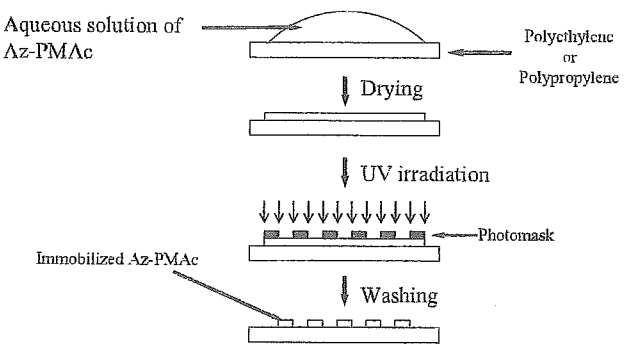

Fig. 2. Schematic illustration of micropatterning procedure.

10 mA. The take-off angle of the photo-electrons was 90°.

2.5. Measurement by atomic force microscopy (AFM)

The measurement was performed using an SPI-3800 (Seiko Instruments Inc., Chiba, Japan). The micropatterned sample was dried in vacuo for 1 day at room temperature and was set in a cell holder into which water could be injected. After observation of the dry sample, distilled water was injected into the sample cell and the same position was observed. The measurement was performed using the tapping mode with a nominal force constant of 0.09 N/m.

2.6. Interaction with proteins

Fluorescein isothiocyanate (FITC)-labeled bovine serum albumin and FITC-labeled immunoglobulin were purchased from Sigma (St. Louis, MO). FITC-labeled fibrinogen was prepared as follows: a phosphate-buffered solution (PBS; 25 ml) containing human fibrinogen (500 μg) was added dropwise to a PBS (25 ml, pH 8.0) containing FITC (12.5 μg) and the pH of the mixture was adjusted to 9.0. The mixture was stirred at room temperature for 2 h. The resulting solution was dialyzed against double-distilled water using a Millipore dialysis tube (cut-off less than 10 000) at 4°C until the release of FITC became undetectable by fluorescence spectroscopy. Finally, the purified protein was lyophilized. All procedures were carried out in darkness.

The protein adsorption experiment was performed as follows: the sample plates were incubated in PBS containing the FITC-labeled albumin (10 mg/ml), FITC-labeled immunoglobulin (2 mg/ml), or the FITC-labeled fibrinogen (10 mg/ml) at 37°C for 10 min. After being washed with PBS, the sample was observed by fluorescence microscopy.

2.7. Interaction with platelets

Human whole blood was collected from healthy volunteers in a disposable syringe containing 3 ml of aqueous solution of 3.8 wt% sodium citrate. The citrated whole blood was immediately centrifuged for 15 min at 1200 rpm to obtain citrated platelet-rich plasma (PRP). The micropatterned sample plates were placed in contact with PRP and left for 60 min at 37°C. The PRP was removed with an aspirator, and the membrane was rinsed three times with PBS. Subsequently, 2.5 vol% glutaraldehyde in PBS was poured into each well containing the sample plates, and the samples were stored at room temperature for 2 h in order to fix the blood components on the sample plate. After it had been rinsed sufficiently with distilled water, the samples were freeze-dried. The surface of the sample plate was observed with a scanning electron microscope (SEM) after gold-sputtering treatment.

2.8. Cell culture

RAW264 (originating from leukemic mouse monocytes) cells were purchased from Riken Cell Bank (Tsukuba, Japan) and were cultured in minimum essential medium (Sigma, St. Louis, MO) with 10% fetal bovine serum and 1% non-essential amino acids (Invitrogen Life Technologies, Carlsbad, CA). The recovered cells were washed with the culture medium and suspended in each medium containing no serum (3×10^5 cells per 60 mm-diameter culture dish). The cell suspension was added to the sample plate, which was sterilized with 70% ethanol. The cells were incubated at 37°C under 5% v/v of CO_2 and were observed by a phase-contrast microscope equipped with a video camera.

3. Results and discussion

3.1. Synthesis of photo-reactive MPC polymer

The UV and fluorescence spectra of Az-PMAc are shown in Fig. 3. In the UV spectrum of the photo-reactive polymer, an absorption at 269 nm, which is assignable to the azidophenyl group, was observed.

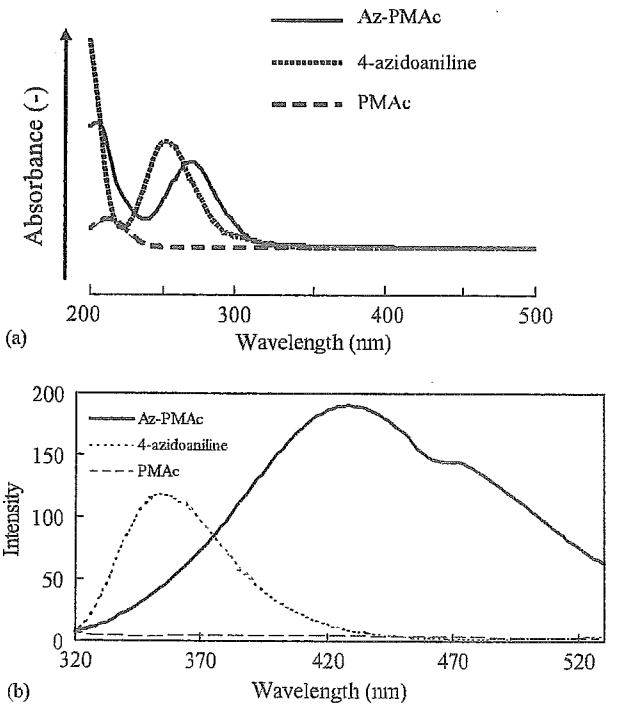

Fig. 3. UV (a) and fluorescence (b) spectra of azidoaniline, PMAc, and Az-PMAc.

Fig. 3a indicates that the absorption was slightly red shifted from the corresponding absorption of 4-azidoaniline, and Fig. 3b shows that the fluorescence was red shifted. These shifts may be due to electron delocalization of the azidophenyl group caused by amide bond formation. In previous studies, the peaks of photo-reactive hyaluronic acid and photo-reactive heparin were also red shifted from 4-azidoaniline [35,37].

3.2. Photo-immobilization

The Az-PMAc was coated on the plates and the coated surface was UV-irradiated with a photo-mask (Fig. 4). The surface pattern was the same as that of the photo-mask. The micropatterned surface was observed by phase-contrast microscopy (Fig. 4b) and by fluorescence microscopy (Fig. 4c). It is known that azido groups are decomposed by UV irradiation, and nitrene groups, which are highly reactive radical groups, are produced. The cast Az-PMAc formed molecular networks as a result of the produced radical groups. In addition, a micropatterned surface was formed both on polyethylene (Fig. 4c) and polypropylene (Fig. 4d) plates. The present result demonstrates that photo-immobilization is useful for covalent immobilization of MPC on various materials.

Previously, Prucker et al. [34] reported photo-chemical attachment of polymer films to solid surfaces via benzophenone derivatives. In their case, the amount of immobilized polymer on the surface reached saturation after about 10–20 min, when the light intensity was 100 mW/cm^2. In the present study, 10 s were enough for preparation of micropatterned immobilization, although the intensity was 16 mW/cm^2. Although the strength of binding of immobilized polymer to the surface has not been investigated, it was demonstrated that 10 s was enough for washing out of non-bound polymers.

The unpatterned PMAc surface on the polyethylene plate was made by UV-irradiation without a photo-mask. XPS measurement of the unpatterned surface demonstrated that the surface was covered with phospholipid polar groups (Fig. 5). In addition to the XPS spectrum of the previously reported MPC polymer coating surface [35,36], a new peak that was ascribed to the amide bond formed by reaction between PMAc and azidoaniline was found at 398 eV.

The water contact angle was measured on the unpatterned surface (Fig. 6). The contact angle on the

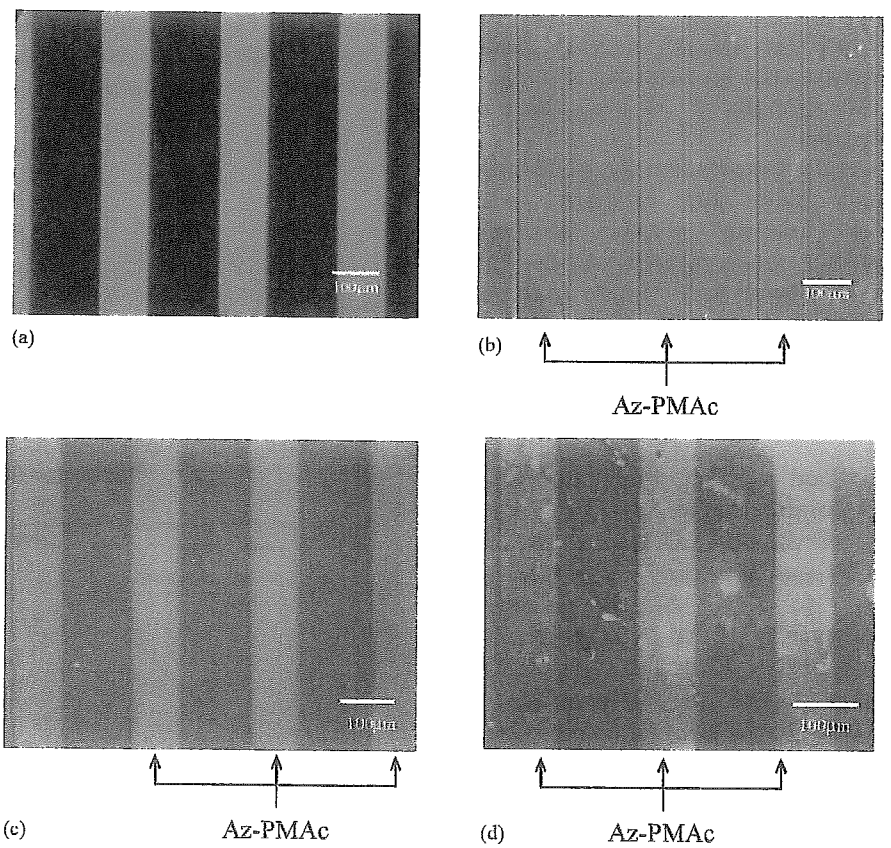

Fig. 4. Phase-contrast micrographs of photo-mask (a); and micropatterned surface of the polyethylene plate (b); fluorescence micrographs of micropatterned surface of the polyethylene plate (c); and of the polypropylene plate (d).

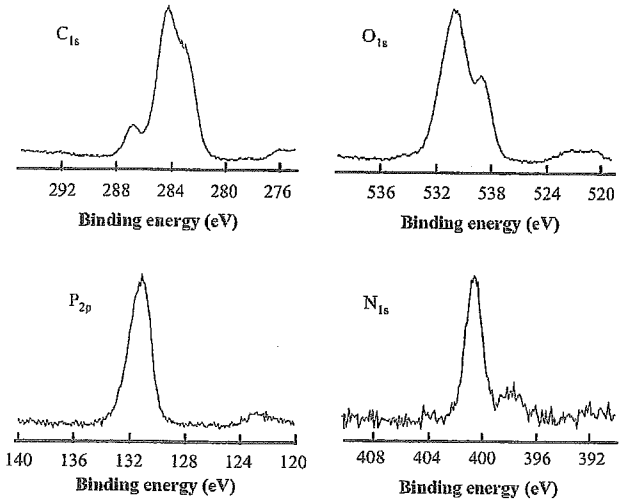

Fig. 5. XPS spectra of the Az-PMAc immobilized polyethylene surface.

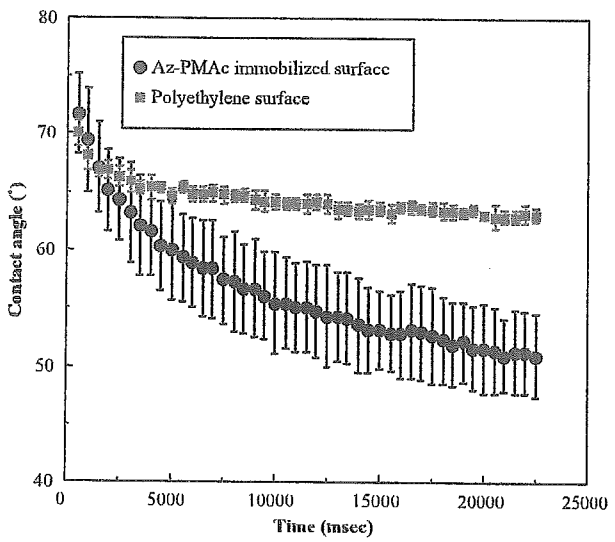

Fig. 6. Time course of static contact angle of water on the Az-PMAc-immobilized and non-immobilized polyethylene surface.

PMAc-immobilized surface rapidly decreased with time, although that on the polyethylene surface did not. It was demonstrated that a hydrophilic surface was formed by immobilization of the PMAc.

The surface was observed by AFM, as shown in Fig. 7. In the dried state, the thickness was about 800 nm. However, the PMAc layer rapidly swelled in water to a thickness of about 4000 nm. The hydrogel state of PMAc was formed after soaking for 10 min in water. Fig. 8 shows the force curves of the micropatterned surface. On the surface of bare polyethylene (2, 4, 6, 8, 10), the force abruptly increased with decreasing distance between the cantilever and the surface. On the other hand, on the Az-PMAc-immobilized region (1, 3, 5, 7, 9) the force did not increase so abruptly with the decrease of distance. These results demonstrated that the Az-PMAc surface was so soft that force was not significantly produced on the surface.

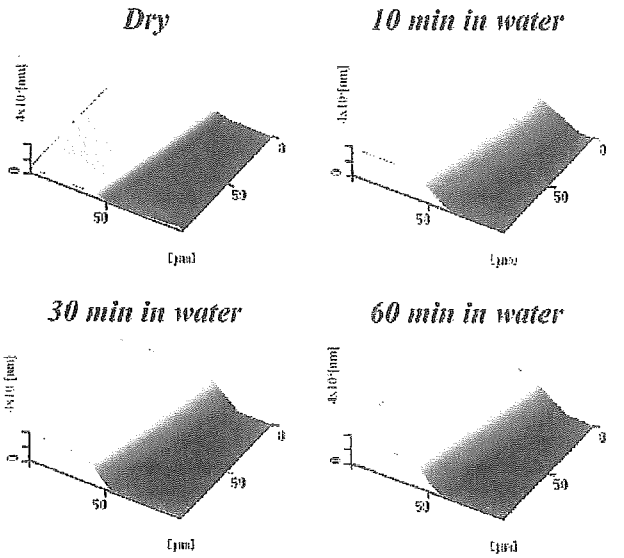

Fig. 7. AFM images of the Az-PMAc-micropatterned surface. The dried sample was measured and then incubated in water for different periods.

3.3. Interaction with biological components

The sample plate was immersed in the protein solutions, and the protein-adsorbed sample was observed by fluorescence microscopy (Fig. 9). Albumin, immunoglobulin, and fibrinogen predominantly adsorbed onto the non-immobilized surface. The fluorescence intensity of adsorbed proteins is significantly higher than that of Az-PMAc alone. Previously, we reported that an MPC-adsorbed surface inhibited adsorption of proteins [37,38]. The present study confirmed the previous reports.

Human blood platelet adhesion onto the micropatterned surface was observed by SEM. The number of platelets on the PMAc-immobilized regions $(0.34 \pm 0.02) \times 10^3$ cell/μm^2 was significantly less than that on the non-immobilized regions $(1.13 \pm 0.12) \times 10^3$ cell/μm^2. The non-adhesiveness of MPC polymer has been reported previously [38]. The present study critically demonstrated this property.

The time course of behavior of RAW264 on the micropatterned surface is shown in Fig. 10. When the cells were added to the surface, they randomly distributed independent of the immobilized material. However, after 5 min, they began to aggregate on the Az-PMAc-immobilized surface; the cellular aggregates increased in size with time and eventually floated. On the

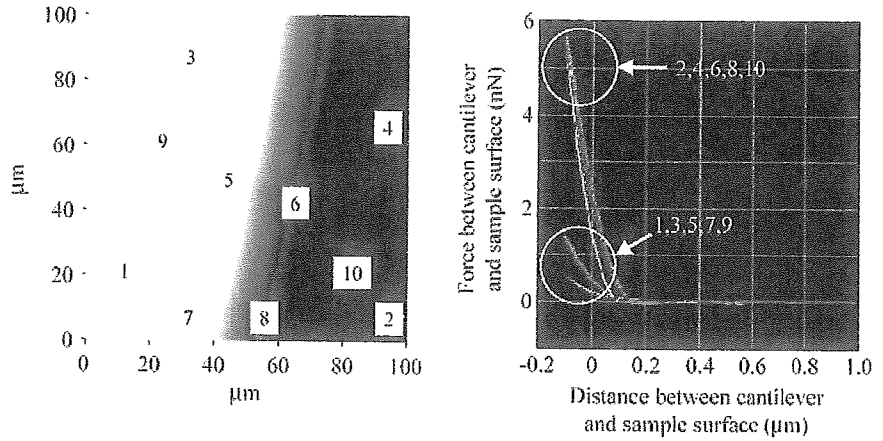

Fig. 8. Contact points of the cantilever with surfaces and the force curve between the cantilever and surfaces. The numbers represent the contact points of the cantilever. Points 1, 3, 5, 7, and 9 were on the Az-PMAc-immobilized surface and points 2, 4, 6, 8, and 10 on the bare polyethylene surface.

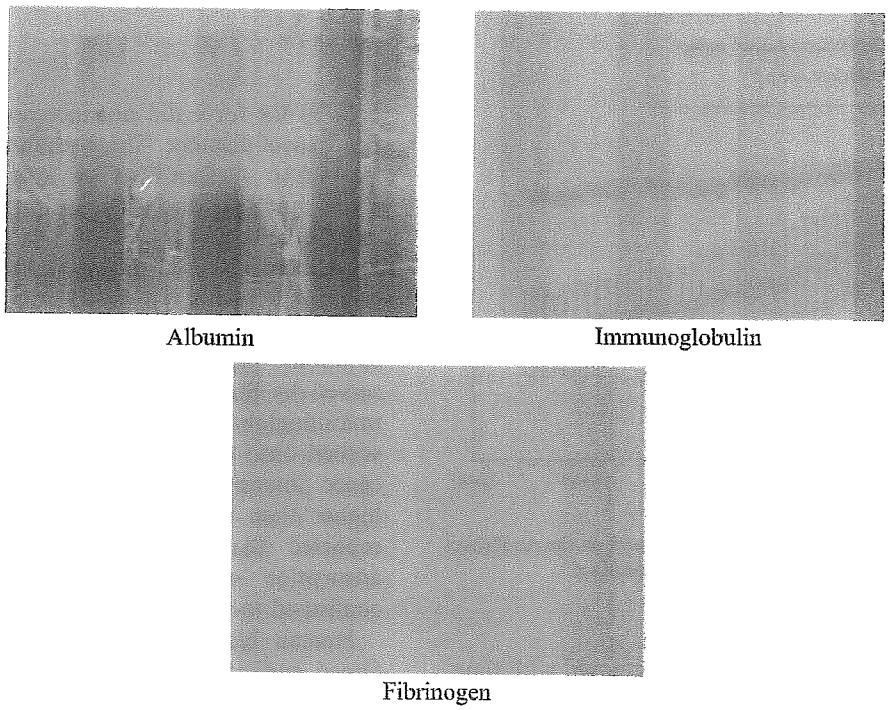

Fig. 9. Fluorescence micrographs of proteins (albumin, immunoglobulin, and fibrinogen) adsorbed onto the Az-PMAc-micropatterned polyethylene surface. The wavelengths of excitation and emission were 470±20 and 525±25 nm, respectively.

non-immobilized region the cells adhered and spread on the surface. The floated aggregates on the Az-PMAc-immobilized region were completely removed by mild shaking. It is known that RAW264 shows macrophage-like properties and tends to adhere to various materials [39]. It was demonstrated that PMAc inhibited the adhesion of even very adhesive cells.

The present study demonstrated photo-immobilization of a phospholipid polymer and visualized the interactions with biocomponents such as proteins, platelets, and cells. The photo-immobilization technique is useful for surface modification and the phospholipid polymer significantly reduced the interactions with proteins and cells.

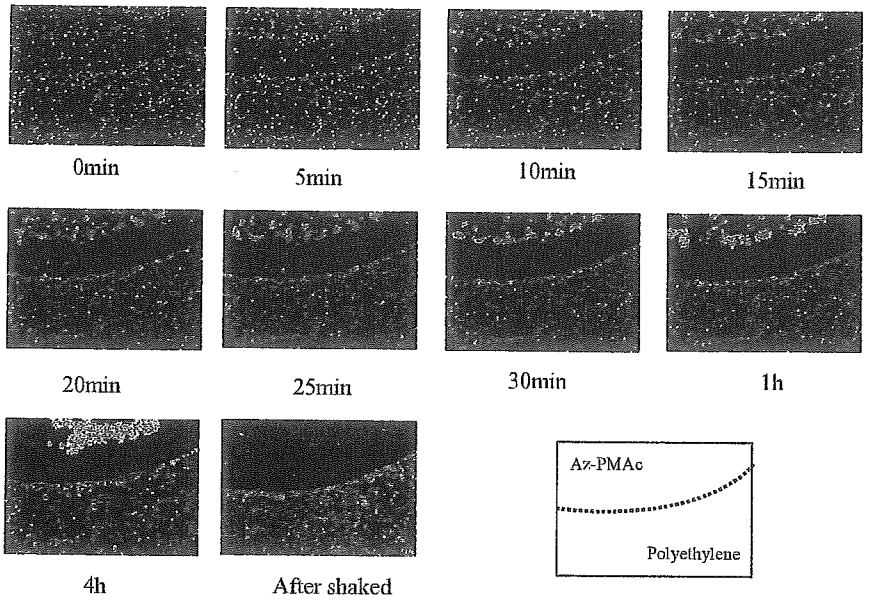

Fig. 10. Time course of behavior of RAW264 cells on Az-PMAc-immobilized and non-immobilized region (polyethylene surface), as observed by phase-contrast microscopy with a video camera.

Acknowledgements

This work was supported in part by a grant from the Japanese Ministry of Education, Culture, Sports, Science, and Technology (14380406). The authors thank Mr. Akihiko Watanabe for his support with the AFM measurement.

References

[1] Shen WW, Boxer SG, Knoll W, Frank C. Polymer-supported lipid bilayers on benzophenone-modified substrates. Biomacromolecules 2001;2:70–9.
[2] Naumann CA, Prucker O, Lehmann T, Rühe J, Knoll W, Frank CW. The polymer-supported phospholipid bilayer: tethering as a new approach to substrate-membrane stabilization. Biomacromolecules 2002;3:27–35.
[3] Mennicke U, Salditt T. Preparation of solid-supported lipid bilayers by spin-coating. Langmuir 2002;18:8172–7.
[4] Devadoss A, Burgess JD. Detection of cholesterol through electron transfer to cholesterol oxidase in electrode-supported lipid bilayer membranes. Langmuir 2002;18:9617–21.
[5] Andersson AS, Glasmästar K, Sutherland D, Lidberg U, Kasemo B. Cell adhesion on supported lipid bilayers. J Biomed Mater Res 2003;64A:622–9.
[6] Richter RP, Brisson A. Characterization of lipid bilayers and protein assemblies supported on rough surfaces by atomic force microscopy. Langmuir 2003;19:1632–40.
[7] Baumgart T, Offenhäuser A. Polysaccharide-supported planar bilayer lipid model membranes. Langmuir 2003;19:1730–7.
[8] Ross EE, Rozanski LJ, Spratt T, Liu S, O'Brien DF, Saavedra SS. Planar supported lipid bilayer polymers formed by vesicle fusion. 1. Influence of diene monomer structure and polymerization method on film properties. Langmuir 2003;19:1752–65.
[9] Sengupta K, Schilling J, Marx S, Fischer M, Bacher A, Sackmann E. Mimicking tissue surfaces by supported membrane coupled ultrathin layer of hyaluronic acid. Langmuir 2003;19:1775–81.
[10] Zhao J, Tamm LK. FTIR and fluorescence studies of interactions of synaptic fusion proteins in polymer-supported bilayers. Langmuir 2003;19:1838–46.
[11] Schneider J, Barger W, Lee GU. Nanometer scale surface properties of supported lipid bilayers measured with hydrophobic and hydrophilic atomic force microscope probes. Langmuir 2003;19:1899–907.
[12] Sun XL, Liu H, Orban JM, Sun L, Chaikof EL. Synthesis and terminal functionalization of a polymerizable phosphatidylethanolamine. Bioconjugate Chem 2001;12:673–7.
[13] Schuster B, Weighert S, Pum D, Sára M, Sleytr UB. New method for generating tetraether lipid membranes on porous supports. Langmuir 2003;19:2392–7.
[14] Elliot JT, Burden DL, Woodward JT, Sehgal A, Douglas JF. Phospholipid monolayers supported on spun cast polystyrene films. Langmuir 2003;19:2275–83.
[15] Ishihara K, Ueda T, Nakabayashi N. Preparation of phospholipids polymers and their properties as polymer hydrogel membrane. Polym J 1990;22:355–60.
[16] Ishihara K, Iwasaki Y. Reduced protein adsorption on novel phospholipids polymers. J Biomater Appl 1998;13:111–27.
[17] Lewis AL, Hughes PD, Kirkwood LC, Leppard SW, Redman RP, Tolhurs LA, Stratford PW. Synthesis and characterization of phosphorylcholine-based polymers useful for coating blood filtration devices. Biomaterials 2000;21:1847–59.
[18] Lewis AL, Cumming ZL, Goreish HH, Kirkwood LC, Tolhurs LA, Stratford PW. Crosslinkable coatings from phosphorylcholine-based polymers. Biomaterials 2001;22:99–111.
[19] Court JL, Redman RP, Wang JH, Leppard SW, O'Byrne VJ, Small SA, Lewis AL, Jones SA, Stratford PW. A novel phosphorylcholine-coated contact lens for extended wear use. Biomaterials 2001;22:3261–72.
[20] Lu JR, Murphy EF, Su TJ, Lewis AL, Stratford PW, Satija SK. Reduced protein adsorption on the surface of a chemically grafted phospholipid monolayer. Langmuir 2001;17:3382–9.

[21] Yoshina-Ishii C, Boxer SG. Arrays of mobile tethered vesicles on supported lipid bilayers. J Am Chem Soc 2003;125:3696–7.
[22] Kam L, Boxer SG. Spatially selective manipulation of supported lipid bilayers by laminar flow: steps toward biomembrane microfluidics. Langmuir 2003;19:1624–31.
[23] Carlson JW, Bayburt T, Sligar SG. Nanopatterning phospholipid bilayers. Langmuir 2000;16:3927–31.
[24] Grooves JT, Mahal LK, Bertozzi CR. Control of cell adhesion and growth with micropatterned supported lipid membranes. Langmuir 2001;17:5129–33.
[25] Orth RN, Wu M, Holowka DA, Craighead HG, Baird BA. Mast cell activation on patterned lipid bilayers of subcellular dimensions. Langmuir 2003;19:1599–605.
[26] Sapuri AR, Baksh MM, Grooves JT. Electrostatically targeted intermembrane lipid exchange with micropatterned supported membranes. Langmuir 2003;19:1606–10.
[27] Matsuda T, Sugawara T. Photochemical protein fixation on polymer surfaces via derivatized phenyl azido group. Langmuir 1995;11:2272–6.
[28] Ito Y. Surface micropatterning to regulate cell functions. Biomaterials 1999;20:2333–42.
[29] Chen G, Ito Y. Gradient micropattern immobilization of EGF to investigate the effect of artificial juxtacrine stimulation. Biomaterials 2001;22:2453–7.
[30] Ito Y, Chen G, Imanishi Y, Morooka T, Nishida E, Okabayashi Y, Kasuga M. Differential control of cellular expression by diffusible and non-diffusible EGF. J Biochem 2001;129:733–7.
[31] Chen G, Ito Y, Imanishi Y, Magnani A, Lamponi S, Barbucci R. Photoimmobilization of sulphated hyaluronic acid for antithrombogenicity. Bioconjugate Chem 1997;8:730–4.
[32] Ito Y, Hayashi M, Imanishi Y. Gradient micropattern immobilization of heparin and its interaction with cells. J Biomater Sci Polym Ed 2001;12:367–78.
[33] Liu H, Ito Y. Gradient-micropattern-immobilization of a thermoresponsive polymer to investigate its effect on cell behaviors. J Biomed Mater Res 2003;67A:1424–9.
[34] Prucker O, Naumann CA, Rühe J, Knoll W, Frank CW. Photochemical attachment of polymer films to solid surfaces via monolayers of benzophenone derivatives. J Am Chem Soc 1999;121:8766–70.
[35] Ishihara K, Tanaka S, Furukawa N, Kurita K, Nakabayashi N. Improved blood compatibility of segmented polyurethanes by polymeric additives having phospholipid polar groups. I. Molecular design of polymeric additives and their functions. J Biomed Mater Res 1996;32:391–9.
[36] Ishihara K, Ishikawa E, Iwasaki Y, Nakabayashi N. Inhibition of fibroblast cell adhesion on substrate by coating with 2-methacryloyloxyethyl phosphorylcholine polymers. J Biomater Sci Polym Ed 1999;10:1047–61.
[37] Iwasaki Y, Fujiike A, Kurita K, Ishihara K, Nakabayashi N. Effect of reduced protein adsorption on platelet adhesion at the phospholipid polymer surfaces. J Biomater Sci Polym Ed 1996;8:151–63.
[38] Iwasaki Y, Ishihara K, Nakabayashi N, Khang G, Jeon JH, Lee JW, Lee HB. Platelet adhesion on the gradient surfaces grafted with phospholipid polymer. J Biomater Sci Polym Ed 1998;9:801–16.
[39] Ito Y, Nogawa M. Preparation of a protein-array using a photoreactive polymer for a cell adhesion assay. Biomaterials 2003;24:3021–6.

Available online at www.sciencedirect.com
SCIENCE DIRECT®
ELSEVIER
Materials Research Bulletin 41 (2006) 515–524
Materials Research Bulletin
www.elsevier.com/locate/matresbu

Enhancement of mechanical strength of TiO_2/high-density polyethylene composites for bone repair with silane-coupling treatment

Masami Hashimoto [a,*], Hiroaki Takadama [a], Mineo Mizuno [a], Tadashi Kokubo [b,1]

[a] *Japan Fine Ceramics Center, 2-4-1 Mutsuno, Atsuta-ku, Nagoya 456-8587, Japan*
[b] *Research Institute for Science and Technology, Chubu University, 1200 Matsumoto-cho, Kasugai 487-8501, Japan*

Received 14 April 2005; received in revised form 7 September 2005; accepted 19 September 2005
Available online 7 October 2005

Abstract

Mechanical properties of composites made up of high-density polyethylene (HDPE) and silanated TiO_2 particles for use as a bone-repairing material were investigated in comparison with those of the composites of HDPE with unsilanized TiO_2 particles. The interfacial morphology and interaction between silanated TiO_2 and HDPE were analyzed by means of Fourier transform infrared (FT-IR) spectroscopy and scanning electron microscopy (SEM). The absorption in spectral bands related to the carboxyl bond in the silane-coupling agent, the vinyl group in the HDPE, and the formation of the ether bond was studied in order to assess the influence of the silane-coupling agent. The SEM micrograph showed that the "bridging effect" between HDPE and TiO_2 was brought about by the silane-coupling agent. The use of the silane-coupling agent and the increase of the hot-pressing pressure for shaping the composites facilitated the penetration of polymer into cavities between individual TiO_2 particles, which increased the density of the composite. Therefore, mechanical properties such as bending yield strength and Young's modulus increased from 49 MPa and 7.5 GPa to 65 MPa and 10 GPa, respectively, after the silane-coupling treatment and increase in the hot-pressing pressure.

Keywords: A. Composites; C. Infrared spectroscopy; D. Mechanical property

1. Introduction

Since the discovery of Bioglass® in the early 1970s [1], various bioactive ceramics, including sintered hydroxyapatite [2] and glass–ceramic A-W containing crystalline apatite and wollastonite ($CaO{\cdot}SiO_2$) [3], have been developed and clinically used as materials, for example, for artificial middle-ear bones, maxillofacial implants, bone fillers, artificial iliac crests, artificial vertebrae, and artificial intervertebral discs. Among them, glass–ceramic A-W shows fracture toughness as high as 2 MPa $m^{1/2}$ [4,5] and high bioactivity [6]. Hence it can be used to replace bones subjected to high loads, such as vertebrae and intervertebral discs [7]. Highly loaded bones such as tibial and femoral bones, however, cannot be replaced even with this glass–ceramic, since its fracture toughness is lower and its elastic modulus is higher than those of natural bone. For these purposes, implants made of metal, such as titanium metal and

* Corresponding author. Tel.: +81 52 871 3500; fax: +81 52 871 3599.
E-mail addresses: masami@jfcc.or.jp (M. Hashimoto), takadama@jfcc.or.jp (H. Takadama), mizuno@jfcc.or.jp (M. Mizuno), kokubo@isc.chubu.ac.jp (T. Kokubo).
[1] Tel.: +81 568 51 6583; fax: +81 568 51 1642.

0025-5408/$ – see front matter
doi:10.1016/j.materresbull.2005.09.014

its alloy, subjected to alkali and heat treatment [8] or alkali, water and heat treatment [9] have been developed. They have, however, much higher elastic moduli than that of natural bone. This is a critical problem in some applications, since the high elastic modulus of these materials may induce resorption of the surrounding bone because of stress shielding. Therefore, highly bioactive materials with mechanical properties analogous to those of natural bone are desired to be developed.

Hydroxyapatite-particle-reinforced high-density polyethylene (HDPE) composite (HAPEX®) was developed in the early 1980s as an analogue for bone [10]. It is already in clinical use as the material of artificial middle-ear bones. Some of the mechanical properties of HAPEX®, such as the tensile strength, have already been confirmed to be suitable for use in the human body [11–13]. However, the fracture toughness and elastic modulus of HAPEX® are lower than those of living bone. Glass–ceramic A-W-reinforced HDPE has been in development since 1998 [14,15]. The bioactivity of this composite is higher than that of HAPEX®, but the mechanical strengths of this composite are lower.

Previous studies by the present authors have shown that TiO_2-nanoparticle-reinforced HDPE composites (hereafter TiO_2/HDPE) exhibit bending strength and Young's modulus analogous to those of natural bone as well as bioactivity [16,17]. The bending strength and Young's modulus were found to vary from almost 28 to 54 MPa and 1.4 to 7.6 GPa, respectively, depending on the TiO_2 content. However, only a very weak mechanical adhesion seemed to exist between constituent phases in these composites. The fracture surface of the TiO_2/HDPE composites showed no residual HDPE on the TiO_2 particles, indicating that no chemical bond existed between TiO_2 and HDPE. Also, there were voids at the particle–matrix interface, resulting in a lower density than the theoretical one.

For incompatible composites containing at least one component, the final mechanical strengths are determined by two competing factors. One is the extent of compatibility between the inorganic filler and the polymer. The other is the presence of voids, cracks and fractures in the interphase between the filler and polymer [18].

The interface between inorganic filler particles and the matrix polymer plays an important role in determining the properties of a composite. Particle–matrix interaction is expected to influence the structure of the composites, mainly through its influence on the dispersion of the filler particles in the matrix [19–21]. Most commonly, the surface of the filler is treated to become more chemically compatible with the polymer matrix. A very common reactive treatment is silane treatment of the fillers [22]. The widespread use of silane treatment can be attributed to the availability of a wide range of endgroups. Thus, the interaction between the inorganic surface and the matrix polymer can be tuned by selecting the appropriate endgroups.

In this work, we focus on the study of composites of HDPE and surface-modified TiO_2, in particular, the adhesion between the two phases. The silane molecule used for surface treatment has the hydrocarbon functional group. The hydrocarbon endgroup is used in coupling agents that interact well with polyolefin, such as polyethylene. Also, the synergistic effects of surface treatment and of the increase of hot-pressing (HP) pressure applied during shaping on mechanical strength were investigated.

2. Experimental

2.1. Materials

Solvents and reagents, all of special reagent grade, were used without further purification. The anatase-type TiO_2 nanopowder was manufactured by Ishihara Sangyo Kaisha, Ltd., Mie, Japan. The median particle size of TiO_2 powders was 535 nm [17]. TiO_2 powders were treated with a silane-coupling agent as follows: 1.1 g of [γ-(methacryloxy)propyl]trimethoxysilane (γ-MPS) (Shinetsu Co. Ltd., Osaka, Japan), 1.6 g of ethanol and 0.2 g of ion-exchanged distilled water were stirred with a magnetic stirrer for 10 min. The solution containing the silane-coupling agent was added to 110 g of TiO_2 powder and mixed in the shaker mixer TURBULA T2F (W. A. Bachofen AG Co., Basel, Switzerland) at 25 °C for 1 h. The rotation speed was 96 rpm. After mixing, the mixtures were dried and heated at 130 °C for 5 min.

HDPE (Japan Polyolefins Co., Ltd., Tokyo, Japan) has the number-average molecular weight (Mn) of 1.21×10^4, weight-average molecular weight (Mw) of 7.67×10^4 and z-average molecular weight (Mz) of 47.6×10^4; Mw/Mn is 6.35 and Mz/Mw is 6.20. The melt flowing rate (MFR) of this polyethylene is 8.

The influence of silanation of TiO_2 nanoparticles on the flow behavior of TiO_2/HDPE compound was evaluated using a computer-controlled torque rheometer, 30C-150 (Toyo Seiki Seisaku-sho, Ltd., Tokyo, Japan). Reaction was performed in a chamber with continuous monitoring of torque. The mixer chamber was initially heated to 210 °C.

HDPE and TiO_2 with and without γ-MPS treatment were introduced into the heated chamber simultaneously. The rotor speed was fixed at 25 rpm. The total mixing process lasted about 30 min.

2.2. Preparation of TiO_2/HDPE composites

The manufacturing process of TiO_2/HDPE with γ-MPS involved kneading and compression molding. The filler content was set at 40 vol% because the composite with this composition shows both bioactivity and mechanical properties analogous to those of human cortical bone [17]. This composite was denoted as TiO_2/HDPE-40. HDPE was dried at 80 °C for 8 h and then kneaded at 210 °C in a batch kneader PBV 0.3 (Irie Shokai, Ltd., Tokyo, Japan). TiO_2 particles were added slowly into the melted HDPE with kneading at 210 °C in air. After adding TiO_2, TiO_2/HDPE compound was kneaded at 25 rpm for 30 min.

The obtained compounds were molded at 230 °C for 1 h and then hot-pressed in air at pressures between 2.5 and 5.8 MPa. TiO_2/HDPE composite without γ-MPS was also produced via the same route for comparison purposes.

2.3. Characterization of TiO_2/HDPE composites

2.3.1. Fourier transform infrared spectroscopy

The spectra of the TiO_2/HDPE-40 composite with and without γ-MPS hot-pressed at 2.5 MPa were analyzed with a FT-IR spectrophotometer FT/IR-550 (JASCO Co., Osaka, Japan). The hot-pressed composite surface was ground and dispersed in a matrix of KBr, followed by compression to consolidate the formation of the pellet. FT-IR spectra were obtained by the KBr pellet method in the wave-number range from 400 to 4000 cm^{-1} with a resolution of 4 cm^{-1}.

2.3.2. SEM observation

The fracture surfaces of TiO_2/HDPE-40 composites with and without γ-MPS hot-pressed at 2.5 MPa were examined using the field emission scanning electron microscope (FE-SEM) JSM-633OF (JEOL DATUM Co. Ltd., Nagoya, Japan) after coating them with a thin Au film.

2.3.3. Mechanical test

Three-point bend testing was performed using five samples of each type of composite. The specimens were cut to the desired shape and then polished, using 400 grit silicon carbide paper, to a size of 40 mm × 10 mm × 4 mm. A testing machine, Model 5582 (Instron Co. Ltd., LA, USA), was used to apply a load over a 30 mm span. Measurements were performed with a cross-head speed of 1.0 mm/min at room temperature, according to JIS K 7171. Bending yield strength was calculated as [14,23]

$$\text{Bending yield strength, } \sigma_f = \left(\frac{3p_f L}{2bd^2}\right)\left(\frac{n+2}{3}\right) \quad (1)$$

p_f is the load at fracture (N), L is the sample length (mm), b is the sample width (mm), d is the sample height (mm), and n is a strain-hardening exponent ($0 < n < 1$). The strain-hardening exponent n was estimated as the slope of log–log plot of p versus δ in the nonlinear region of the load–displacement curve. δ is the deflection of the specimen at mid-span (mm).

The Young's modulus was estimated from the slope of the initial linear elastic region of the load–displacement curve.

2.3.4. Density

The density of TiO_2/HDPE-40 composite was measured by the Archimedes method using a pycnometer and a glass bottle of known volume with a capillary tube at the top as a container. The liquid medium was distilled water for all materials.

3. Results

3.1. Torque of composites

It is known that melt viscosity can be related to the torque measured by the equipment during blending [24]. Fig. 1 shows a plot of torque versus time for TiO_2/HDPE-40 with (a) and without (b) γ-MPS. The introduction of cold HDPE

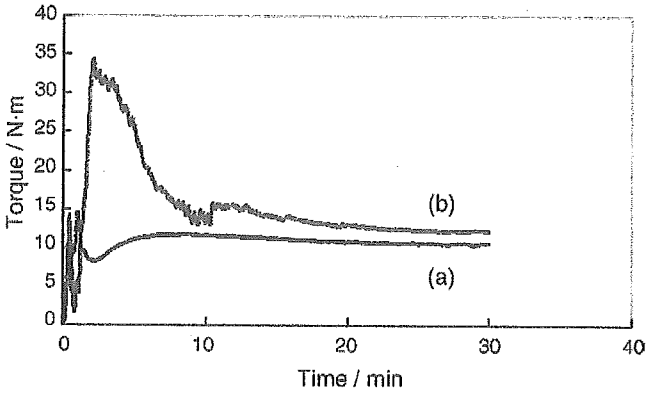

Fig. 1. Plot of torque vs. time for TiO_2/HDPE-40 composites with (a) and without (b) γ-MPS at 200 °C.

and TiO_2 into the preheated mixer chamber initially led to an increase of torque, followed by a decrease of torque during the fusion of HDPE (Fig. 1(a) and (b)). The torque of TiO_2/HDPE-40 without γ-MPS became approximately constant after about 10 min (Fig. 1(b)). On the other hand, the system containing γ-MPS showed lower and variable torque during experiments (Fig. 1(a)). The addition of γ-MPS decreased the torque during the first 2–3 min due to the plasticizing effect of the silanized TiO_2. This torque slowly increased with processing, probably due to chain branching reactions induced by heat and mechanical forces. The torque of TiO_2/HDPE-40 composite with γ-MPS was lower than that of composite without γ-MPS after blending for 30 min. Therefore, a silane-coupling agent such as γ-MPS produced a lower viscosity TiO_2/HDPE-40 composite, as can be seen from curve (a).

3.2. FT-IR spectra of composites

Fig. 2 shows the characteristic spectra of TiO_2/HDPE-40 with (a) and without (b) γ-MPS. It shows the bands involved in the interfacial interaction between the TiO_2 particles and the HDPE matrix in the presence or absence of γ-MPS. Upon comparing the composite spectra, differences in the shape and position of the bands can be observed.

The most significant bands of the TiO_2 particles studied and the assignment for each one are a broad adsorption band between 500 and 1000 cm^{-1} attributed to Ti–O–Ti linkages in TiO_2 nanoparticles [25,26]. On the other hand, in the HDPE spectrum, it is necessary to highlight the band at 1474 cm^{-1} ($-CH_2$) [27] and the characteristic band at 1386 cm^{-1} (wagging $-CH_2$) [27]. In Fig. 2, one special band at 1720 cm^{-1} and a slightly different shape at 900–1300 cm^{-1}, corresponding to neither TiO_2 particles nor HDPE, are observed only for the composite with γ-MPS (a). Also, the bands at 3085 cm^{-1} and 3025 cm^{-1} are observed for the composite without γ-MPS (b).

Fig. 3 shows the FT-IR spectra in the 1300–2000 cm^{-1} region of the TiO_2/HDPE-40 composite hot-pressed at 2.5 MPa with (a) and without (b) γ-MPS. As shown in Fig. 3(a), the spectral band at 1720 cm^{-1} was attributed to the carboxyl group of γ-MPS. This result indicates the applicability of silane coupling on the surface of TiO_2 particles. The spectral band at 1654 cm^{-1} corresponds to water absorption due to the hydrophilic character of the TiO_2 particles (Fig. 3(a) and (b)).

Fig. 4 shows the FT-IR spectra in the 900–1300 cm^{-1} region of the TiO_2/HDPE-40 composite hot-pressed at 2.5 MPa with (a) and without (b) γ-MPS. The spectral band at 1162 cm^{-1} was attributed to an ether bond (C–O–C). Also, two broad bands appear at 1106 and 1035 cm^{-1}, which are assigned to Si–O stretching vibration, indicating the generation of a Si–O–Si network [28]. The absorption peak at about 940 cm^{-1} corresponds to Si–O–Ti stretching vibration [29,30].

Fig. 5 shows the FT-IR spectra in the 2700–3300 cm^{-1} region of the TiO_2/HDPE-40 composite hot-pressed at 2.5 MPa with (a) and without (b) γ-MPS. The 2946 cm^{-1} band is assigned to the symmetric stretching of CH_2 in HDPE for composites containing 40 vol% of TiO_2 (Fig. 5(a) and (b)). The bands at 3085 and 3025 cm^{-1}, corresponding to the bending of the vinyl group in HDPE, are reduced in the case of TiO_2/HDPE-40 with γ-MPS (Fig. 5(a)).

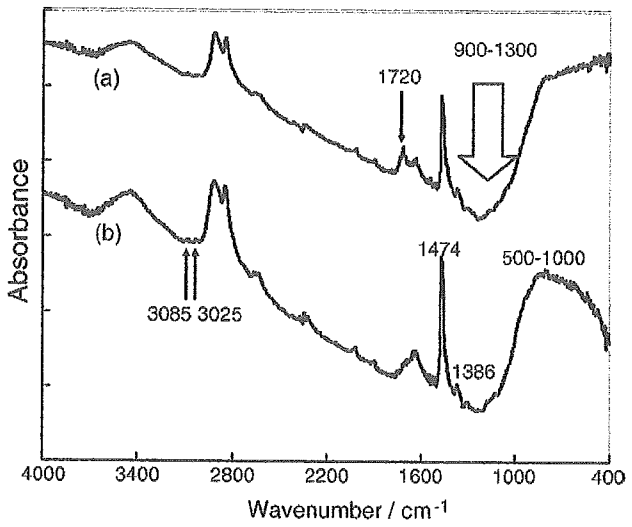

Fig. 2. FT-IR spectra of TiO_2/HDPE-40 composites with (a) and without (b) γ-MPS.

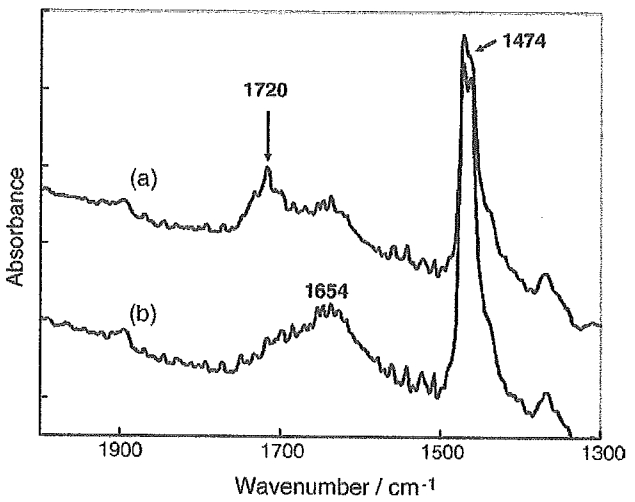

Fig. 3. FT-IR spectra in the 1300–2000 cm^{-1} region for TiO_2/HDPE-40 composites with (a) and without (b) γ-MPS.

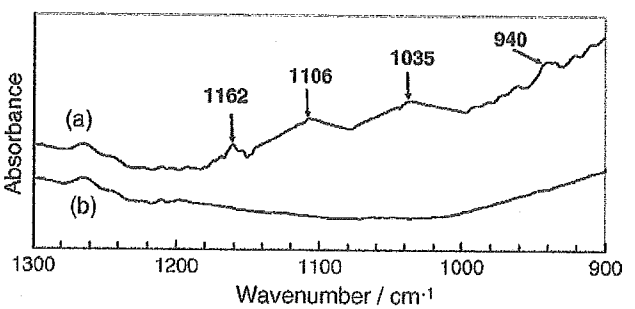

Fig. 4. FT-IR spectra in the 900–1300 cm^{-1} region for TiO_2/HDPE-40 composites with (a) and without (b) γ-MPS.

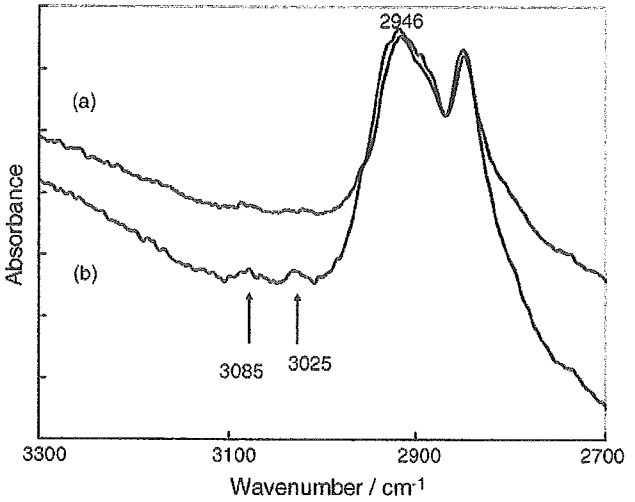

Fig. 5. FT-IR spectra in the 2700–3300 cm^{-1} region for TiO_2/HDPE-40 composites with (a) and without (b) γ-MPS.

3.3. SEM characterization of composites

Fig. 6 shows FE-SEM images of the fracture surfaces of TiO_2/HDPE-40 with (a) and without (b) γ-MPS after the bending test. This figure shows the effect of a tensile load on local deformation of HDPE around the TiO_2 particles in each of the composites. As the FE-SEM image in Fig. 6(a) shows, HDPE covered the surface of individual TiO_2 particles, indicating that a chemical bond existed between TiO_2 and HDPE. However, for TiO_2/HDPE without γ-MPS (Fig. 6(b)), no residual HDPE was found on the TiO_2 particles.

3.4. Mechanical properties of composites

The bending yield strength and Young's modulus of TiO_2/HDPE-40 with (a) and without (b) γ-MPS as a function of hot-pressing (HP) pressure are shown in Figs. 7 and 8, respectively. In the case of TiO_2/HDPE-40 without γ-MPS, the bending yield strength and Young's modulus were independent of HP pressure (Figs. 7(b) and 8(b)). On the other hand, the bending yield strength and Young's modulus of TiO_2/HDPE-40 with γ-MPS increased with increasing HP pressure up to 5 MPa and decreased at pressures higher than 5.7 MPa. The bending yield strength and Young's modulus, respectively, were 49 MPa and 7.5 GPa for the HP pressure of 2.5 MPa, 58 MPa and 8 GPa for the HP pressure of 4.5 MPa, 65 MPa and 10 GPa for the HP pressure of 5 MPa, and 61 MPa and 7 GPa for the HP pressure of 5.7 MPa.

The representative load–displacement curves were obtained for HDPE, and TiO_2/HDPE-40 without (Fig. 9) and with γ-MPS (Fig. 10) by three-point bend testing. Pure HDPE did not fracture within the limits of the three-point

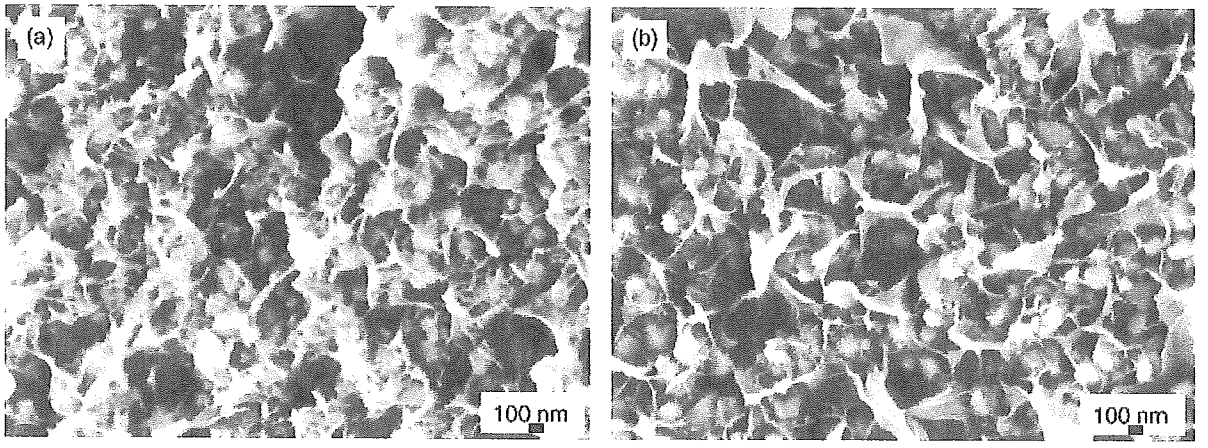

Fig. 6. Scanning electron micrographs of fracture surfaces of TiO_2/HDPE-40 composites with (a) and without (b) γ-MPS.

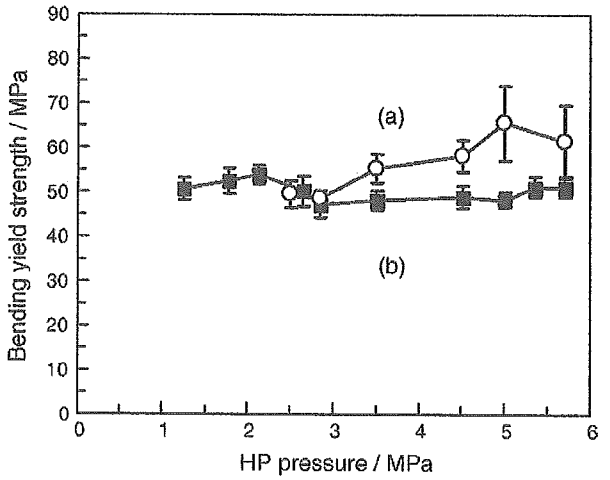

Fig. 7. Bending yield strength of TiO_2/HDPE-40 composites with (a) and without (b) γ-MPS as a function of hot-pressing pressure.

bending apparatus. This behavior indicated the mechanical properties of low bending yield strength and Young's modulus, and large strain to failure. For TiO_2/HDPE-40 without γ-MPS (Fig. 9), it can be noted that all the curves exhibit nearly linear behavior independent of HP pressure. All the composites break in a brittle manner when the load reaches a maximum. However, for TiO_2/HDPE-40 with γ-MPS (Fig. 10), all the curves exhibit the non-linear behavior of a ductile matrix. Once the load reaches its maximum value there are clearly significant differences in the way these

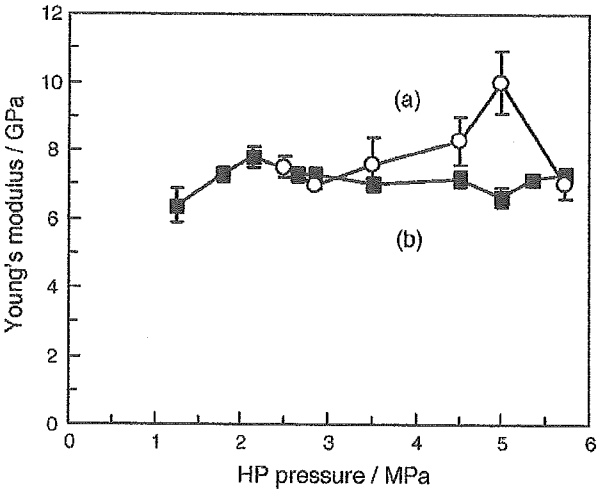

Fig. 8. Young's modulus of TiO_2/HDPE-40 composites with (a) and without (b) γ-MPS as a function of hot-pressing pressure.

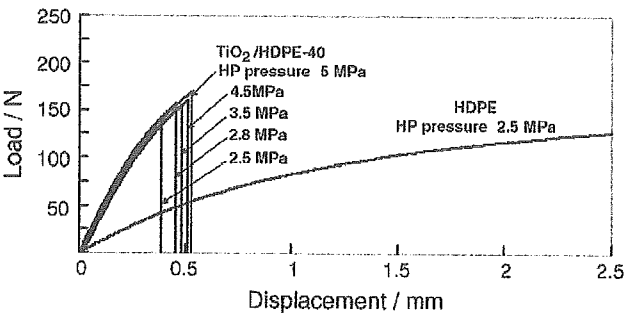

Fig. 9. Load–displacement curve of TiO_2/HDPE-40 composite without γ-MPS hot-pressed at various pressures and that of pure HDPE.

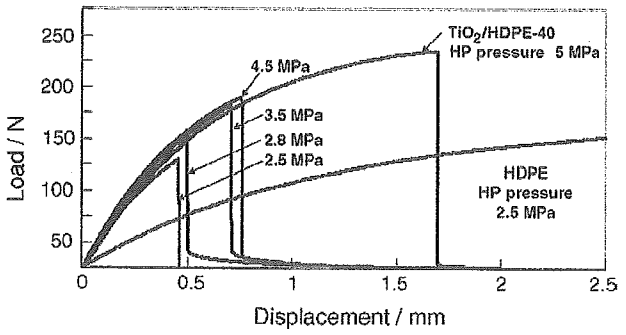

Fig. 10. Load–displacement curve of TiO_2/HDPE-40 composite with γ-MPS hot-pressed at various pressures and that of pure HDPE.

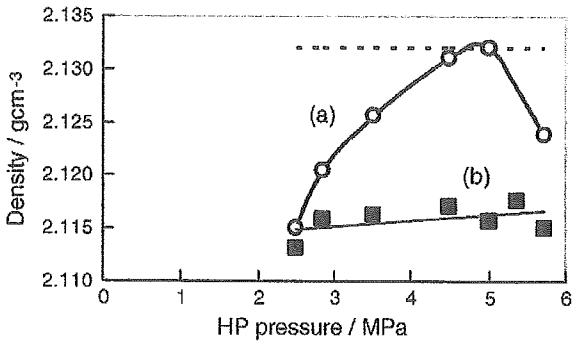

Fig. 11. Density of TiO_2/HDPE-40 composite with (a) and without (b) γ-MPS as a function of pressure applied during shaping (dotted line represents the theoretical density value of 2.132 g/cm^3).

curves decrease. The load–displacement curve depicts a weakly bonded interphase after the interphase fails (HP pressure 2.5 MPa). The TiO_2 particles were separated from the matrix in a controlled manner and friction was measured until all TiO_2 particles were completely removed (HP pressure: 2.8, 3.5 and 4.5 MPa). Fig. 10 shows that the load–displacement curve for silane-treated composite (HP pressure 5 MPa) indicates a very strongly bonded interphase; the interface failed immediately after complete TiO_2 particle separation.

3.5. Density of composites

Fig. 11 shows the densities of the TiO_2/HDPE-40 composites with (a) and without (b) γ-MPS as a function of HP pressure. Compared with the theoretical density (denoted by the dotted line), which was calculated using the rule of mixture, the density of TiO_2/HDPE with γ-MPS (a) increased with HP pressure up to almost identical value to the theoretical one (2.132 g/cm^3) at 5 MPa. However, as the hot-pressing pressure was increased to 5.7 MPa, the discrepancy between the measured and theoretical densities increased. In contrast, the density of TiO_2/HDPE without γ-MPS (b) was independent of HP pressure.

4. Discussion

The mechanical strength of TiO_2/HDPE-40 was enhanced by both the silanation of TiO_2 and the increase of the HP pressure applied to shape the composite.

The TiO_2/HDPE composite without γ-MPS presents very weak physicomechanical adhesion, as shown in Fig. 6(b). For the fracture surface of the TiO_2/HDPE composite, no residual HDPE was found on the TiO_2 particles, indicating that no chemical bond existed between the matrix and filler. Therefore, the voids form at the particle–matrix interface, first in the direction of the applied stress. This void then grows and merges as shear stresses deform the rest of the matrix, leading to the eventual failure of the composites. This result was consistent with the model proposed by Juhasz et al. for an apatite–wollastonite-reinforced HDPE composite with no interfacial bonding [15]. Hence stress transfer

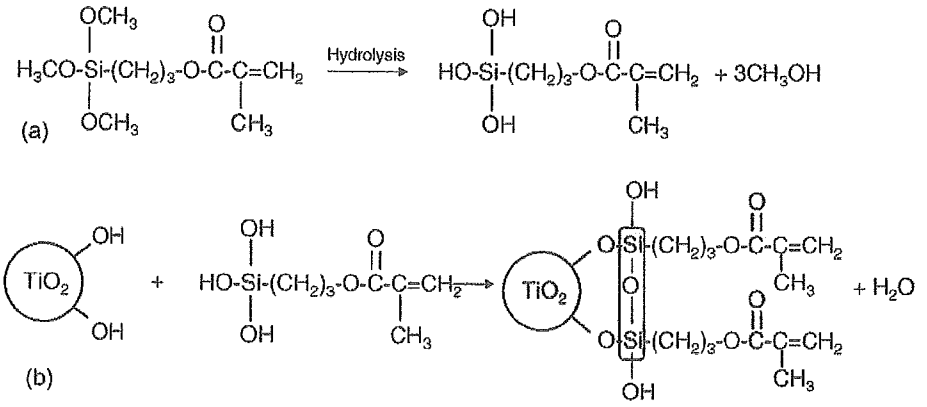

Fig. 12. Scheme of hydrolyzation of γ-MPS and absorption of hydrolyzed alkoxysilanol on TiO_2.

does not take place between TiO_2 and HDPE. On the other hand, for the silanated TiO_2/HDPE composite, as shown in Fig. 6(a), the silane-coupling agent facilitates direct contact between the TiO_2 particles and the HDPE matrix to a higher degree than the contact in the untreated composite. It can also be observed that the composites broke due to shear yield and tearing. The differences between the failure surfaces of differently treated composites are attributed to the different chemical natures of the coupling agent and the different adhesion mechanisms.

In the silanated TiO_2/HDPE composite, as shown in Fig. 4(a), the bands of 1035 and 1106 cm^{-1} are mainly attributed to Si–O–Si vibration. The silane-coupling agent undergoes chemical changes during hydrolysis and drying. During hydrolysis of the silane, the $SiOCH_3$ group will transform into SiOH, as shown in Fig. 12(a). Then, the hydrolyzed alkoxysilanol can be absorbed into the surface and condenses with the hydroxyl group of TiO_2 components, as shown in Fig. 12(b). The hydrolyzed alkoxy silanes can undergo condensation and bond formation. Besides these reactions of the silanol and the hydroxyl groups of the TiO_2 surface, the formation of the siloxane structure can also occur, which gives rise to the band at 940 cm^{-1} attributed to Si–O–Ti (Fig. 4(a)). This reveals the formation of a covalent bond between the silane-coupling agent and the TiO_2 particles.

Fig. 5 shows the evolution of the reduced absorbance corresponding to the bending of the vinyl group (–CH=CH_2, 3025 and 3085 cm^{-1}). This seems to correspond to the reactivity between the double bond of HDPE and those of the coupling agent on TiO_2 particles, as shown in Fig. 13. Therefore, HDPE covered the surface of individual TiO_2 particles, as shown in Fig. 6(a).

Homogeneous dispersion of nanoparticles in a polymeric matrix is very difficult due to the strong tendency of nanoparticles to agglomerate. Consequently, the so-called nanoparticle-filled polymers sometimes contain a number of loosened clusters of particles. It can be seen that in the silane-treated composite, HDPE penetrated into the cavity between TiO_2 particles because of its low viscosity in the molten state (Fig. 1). This seems to indicate that wetting of the TiO_2 particles plays a key role in TiO_2 and HDPE matrix adhesion because it increases the degree of mechanical

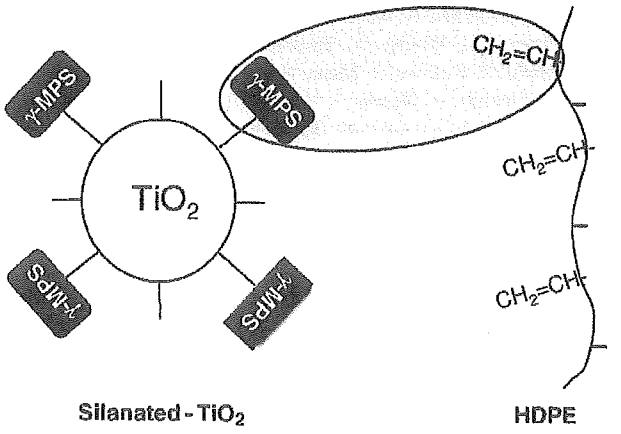

Fig. 13. Adhesion mechanism for silane-treated TiO_2 and HDPE.

interlocking. This means that proper TiO_2 wetting by γ-MPS and an increased hot-pressing pressure could explain the increment of the density of the composites (Fig. 11(a)).

These studies revealed that the final mechanical strengths are determined by two competing factors: one is the increase in compatibility between TiO_2 and HDPE due to the presence of the silane-coupling agent, and the other is the increase in the density of the composite. Also, with high strain (pressure applied during shaping is higher than 5 MPa), the properties of the composite seemed to be deteriorated because high strain leads to the formation of cracks and fractures at interphase boundaries. Therefore, the mechanical strengths of TiO_2/HDPE composite decreased due to the decrease of density.

5. Conclusions

The bending yield strength and Young's modulus increased with the increase of the pressure applied during shaping only for the silane-treated TiO_2/HDPE composite (maximum bending yield strength = 65 MPa, Young's modulus = 10 GPa). γ-MPS has a higher capacity to form the covalent bond, that is, an ether bridge (1162 cm^{-1}). The vinyl groups of HDPE reacted with the double bonds within γ-MPS. Increasing the pressure applied during shaping resulted in an increase in the density of silane-treated TiO_2/HDPE composite. These chemical interactions between TiO_2 and HDPE and the disappearance of voids and cracks resulted in better mechanical performance of silane-treated TiO_2/HDPE composite.

Acknowledgement

This work is supported in part by the National Research and Development Programs for Medical and Welfare Apparatus entrusted by the New Energy and Industrial Technology Development Organization (NEDO) to the Japan Fine Ceramics Center.

References

[1] L.L. Hench, R.J. Splinter, W.C. Allen, T.K. Greenlee Jr., J. Biomed. Mater. Res. 2 (1971) 117–141.
[2] M. Jarcho, J.L. Kay, R.H. Gumaer, H.P. Drobeck, J. Bioeng. 1 (1977) 79–92.
[3] T. Kokubo, M. Shigematsu, Y. Nagashima, M. Tashiro, T. Nakamura, T. Yamamuro, S. Higashi, Bull. Inst. Chem. Res. Kyoto Univ. 60 (1982) 260–268.
[4] T. Kokubo, S. Ito, M. Shigematsu, S. Sakka, T. Yamamuro, J. Mat. Sci. 20 (1985) 2001–2004.
[5] T. Kokubo, S. Ito, M. Shigematsu, S. Sakka, T. Yamamuro, J. Mat. Sci. 22 (1987) 4067–4070.
[6] K. Ono, T. Yamamuro, T. Nakamura, T. Kokubo, Biomaterials 11 (1990) 265–271.
[7] T. Yamamuro, J. Shikata, H. Okumura, T. Kitsugi, Y. Kakutani, T. Matsui, T. Kokubo, J. Bone Joint Surg. 72-B (1990) 889–893.
[8] H.M. Kim, F. Miyaji, T. Kokubo, T. Nakamura, J. Biomed. Mater. Res. 32 (1996) 409–417.
[9] M. Uchida, H.M. Kim, T. Kokubo, S. Fujibayashi, T. Nakamura, J. Biomed. Mater. Res. 63 (5) (2002) 522–530.
[10] W. Bonfield, M.D. Grynpas, A.E. Tully, J. Bowman, J. Abram, Biomaterials 2 (1981) 185–186.
[11] M. Wang, R. Joseph, W. Bonfield, Biomaterials 19 (1998) 2357–2366.
[12] M. Wang, W. Bonfield, Biomaterials 22 (2001) 1311–1320.
[13] M. Wang, Biomaterials 24 (2003) 2133–2151.
[14] J.A. Juhasz, S.M. Best, W. Bonfield, M. Kawashita, N. Miyata, T. Kokubo, T. Nakamura, J. Mater. Sci.—Mater. Med. 14 (2003) 489–495.
[15] J.A. Juhasz, S.M. Best, R. Brooks, M. Kawashita, N. Miyata, T. Kokubo, T. Nakamura, W. Bonfield, Biomaterials 25 (2004) 949–955.
[16] H. Takadama, M. Hashimoto, Y. Takigawa, M. Mizuno, Y. Yasutomi, T. Kokubo, Key Eng. Mater. 254–256 (2004) 569–572.
[17] M. Hashimoto, H. Takadama, M. Mizuno, T. Kokubo, J. Mater. Sci.—Mater. Med., Submitted for publication.
[18] S. Jose, A.S. Aprem, B. Trancis, M.C. Chandy, P. Werner, V. Alstaedt, S. Thomas, Eu. Polym. J. 40 (2004) 2105–2115.
[19] B. Pukanszky, E. Fekete, F. Tudos, Chemie Macromolecular Symposia 28 (1989) 165–186.
[20] J. Jancar, J. Kucera, Polym. Eng. Sci. 30 (12) (1990) 707–713.
[21] J. Jancar, J. Kucera, Polym. Eng. Sci. 30 (12) (1990) 714–720.
[22] E.P. Plueddemann, Silane Coupling Agents, 3rd ed., Plenum Press, New York, 1991.
[23] N.E. Dowling (Ed.), Engineering Materials For Deformation, Fracture and Fatigue, Prentice-Hall Inc., Englewood Cliffs, NJ, 1993, pp. 570–617 (Chapter 13).
[24] F.W. Fabris, F.C. Stedile, R.S. Mauler, S.M.B. Nachtigall, Eu. Polym. J. 40 (2004) 1119–1126.
[25] C. Xie, Z. Xu, Q. Yang, B. Xue, Y. Du, J. Zhang, Mater. Sci. Eng., B 112 (2004) 34–41.
[26] T. Bezrodna, G. Puchkovska, V. Shymanovska, J. Baran, H. Ratajczak, J. Mol. Struct., in press.
[27] X. Colom, F. Carrasco, P. Pages, J. Canavate, Compos. Sci. Technol. 63 (2003) 161–169.
[28] B.B. Johnsen, K. Olafsen, A. Stori, Int. J. Adhes. Adhes. 23 (2003) 155–163.
[29] B. Bai, J. Zhao, X. Feng, Mater. Lett. 57 (2003) 3914–3918.
[30] G. Gu, Z. Zhang, H. Dang, Appl. Surf. Sci. 221 (2004) 129–135.

Phospholipid polymer surfaces reduce bacteria and leukocyte adhesion under dynamic flow conditions

Jasmine D. Patel,[1] Yasuhiko Iwasaki,[2] Kazuhiko Ishihara,[3] James M. Anderson[1,4]
[1]*Department of Biomedical Engineering, Case Western Reserve University, Cleveland, Ohio 44106*
[2]*Institute of Biomaterials and Bioengineering, Tokyo Medical and Dental University, 2-3-10 Kanda-urugadai, Chiyoda-ku, Tokyo 101-0062, Japan*
[3]*Department of Materials Engineering, School of Engineering, The University of Tokyo, 7-3-1 Hongo, Bukyo-ku, Tokyo 113-8656, Japan*
[4]*The Institute of Pathology, Case Western Reserve University, 2085 Adelbert Road, Room 306, Cleveland, Ohio 44106*

Received 20 December 2004; accepted 3 January 2005
Published online 30 March 2005 in Wiley InterScience (www.interscience.wiley.com). DOI: 10.1002/jbm.a.30302

Abstract: Persistence of infection can occur when the host immune response is compromised because of the presence of a foreign implant. Surface modification of biomaterials with phospholipid polymers may enhance biocompatibility and reduce incidence of infection by impeding bacterial and leukocyte adhesion. A rotating disk model, which generates shear stress from 0 to 18 dynes/cm^2, was used to characterize adhesion of neutrophils, monocytes, and bacteria in phosphate-buffered saline (PBS) or 25% human serum on polyethylene terephthalate surfaces coated with a phospholipid polymer, poly[ω-methacryloyloxyalkyl phosphorylcholine (MAPC)-*co*-*n*-butyl methacrylate (BMA)]. The material designated PMB30 contains a methylene chain length, $(CH_2)_n$, of $n = 2$, whereas PMHB30 contains a chain length of $n = 6$. In PBS, bacterial adhesion was shear stress dependent with the lowest bacterial density observed on PMB30. However, the presence of serum proteins eliminated shear stress and surface chemistry effects in addition to bacterial adhesion reduced to <10% of adhesion in PBS. Trends for leukocyte adhesion in serum demonstrated shear dependence with PMB30 exhibiting the lowest cell density throughout the range of shear stresses. In conclusion, modification of the polyethylene terephthalate surfaces with phospholipid polymers resulted in reduced bacterial and leukocyte adhesion. Furthermore, shortening the methylene chain length of the MAPC copolymer most effectively reduced adhesion. © 2005 Wiley Periodicals, Inc. J Biomed Mater Res 73A: 359–366, 2005

Key words: infection; shear stress; phospholipid polymers; *Staphylococcus epidermidis*; leukocytes

INTRODUCTION

Infection is a serious complication associated with implanted medical devices. Coagulase-negative staphylococci, in particular, *Staphylococcus epidermidis*, are among the most common bacteria isolated from infected implants. Persistence of infection can occur when the host immune response is compromised because of the presence of a foreign implant and the high resistance of biomaterial-adherent bacteria to antibiotic therapy.[1–4]

Infection develops from initial bacterial adhesion on the surface of the implant, followed by bacterial aggregation, proliferation, and exopolysaccharide slime production.[5] Biofilm formation, more specifically the barrier of slime, contributes to the pathogenicity of indwelling device infection by impeding access of leukocytes and antibiotics to the adherent bacteria.[2,6] Therefore, it is critical to inhibit initial bacterial adhesion to biomaterials to prevent the development of chronic infection.

Cardiovascular implants are exposed to a range of shear stress generated by blood flow. Adhesion of cells and bacteria on the biomaterial surface is in part mediated by these shear forces which may contribute to the persistence of device-centered infection. Previous studies have shown that *S. epidermidis* is capable of adhesion on polyetherurethane ureas under shear stress levels as high as 70 dynes/cm^2 and is independent of shear stress.[7] In contrast, leukocyte adhesion on polyetherurethane ureas is sensitive to shear stress and minimal at levels of shear stress >7 dynes/cm^2.[8–10] As a result, leukocytes would be unable to interact with bacteria because of the lack of leukocyte

Correspondence to: Y. Iwasaki; e-mail: yasu.org@tmd.ac.jp
Contract grant sponsor: National Institutes of Health; contract grant number: EB-00279

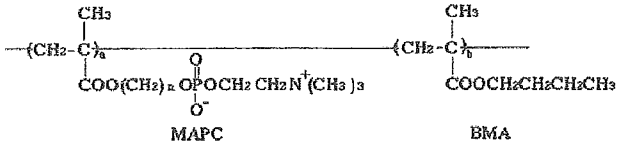

Figure 1. Chemical structure of phospholipids polymers coated onto PET sheets.

adhesion at shear stresses >7 dynes/cm^2 permitting bacteria to colonize on biomaterials.

To facilitate the success of a biomaterial, polymer surfaces can be modified with poly[ω-methacryloyloxyalkyl phosphorylcholine (MAPC)-*co*-*n*-butyl methacrylate (BMA)] to influence material properties and potentially reduce adherent bacteria. At the same time, these surface properties can direct leukocyte adhesion onto the surface, which may also contribute to persistence of biomaterial infection. Poly[2-methacryloyloxyethyl phosphorylcholine (MPC)-*co*-BMA] (PMB) was created to mimic biological membranes that do not cause cell and blood protein adsorption or activation upon contact.[11,12] The MAPC copolymers have been shown to reduce platelet adhesion and activation[13–15] as well as suppress an inflammatory response of adherent cells.[16,17] The excellent compatibility of these materials has been correlated to a strong affinity for phospholipids from human plasma and low protein adsorption.[18–24]

In this study, the effects of the phospholipid polymer surfaces on the adhesion of bacteria and leukocytes under dynamic flow conditions were examined to further elucidate the mechanisms of persistent biomaterial infection. MAPC copolymers were synthesized to contain varying methylene chain lengths, which is the spacer connecting the phosphorylcholine group. Therefore, the effect of the chemical structure of the phosphorylcholine moiety on bacterial and leukocyte adhesion was evaluated.[13]

MATERIALS AND METHODS

Phospholipid polymers surfaces

Polyethylene terephthalate (PET) surfaces were coated with a phospholipid polymer, MAPC-*co*-BMA, in a 0.3 mole fraction of the MAPC unit (Fig. 1). Copolymerization of MAPC and BMA was performed in an ethanol solution with α,α'-azobisisobutyronitrile (AIBN) as an initiator. The phospholipid polymer materials used in this study contained varying methylene chain lengths between the phospholipid polar head and the backbone in the MAPC segment. The material designated poly($MPC_{0.3}$-*co*-$BMA_{0.7}$) (PMB30) contains a methylene chain length, $(CH_2)n$, of n = 2, whereas poly[6-methacryloyloxyhexyl phosphorylcholine ($MHPC)_{0.3}$-*co*-$BMA_{0.7}$] (PMHB30) contains a chain length of n = 6 (Table I). The PET-based materials were cut into 17-mm discs, cleaned with distilled water, sterilized with ethylene oxide gas, and equilibrated in phosphate-buffered saline (PBS) overnight.

Rotating disk system (RDS)

The RDS (Pine Instrument Company) provides a useful *in vitro* model to study cell–biomaterial interactions under well-defined flow fields, which has been detailed in previous studies.[8,25] Based on the radial distance from the center of the disk surface, the system generates a range of shear stress across the surface of the material. Fluid approaches the surface of the disk with constant mass flux which transports the cells or bacteria uniformly to the rotating surface, independent of the radial position. Nearing the surface, the velocity of the fluid is increased proportional to the angular velocity of the disk. Consequently, shear stress is zero at the center of the disk and reaches a maximum at the edges.[26,27]

Components of the RDS were sterilized before conducting any experiments. Previously cut phospholipid polymer surfaces were mounted to stainless steel discs and immersed into the test media maintained at 37°C. The material was rotated at 350 rpm to generate shear stress levels of 0–18 dynes/cm^2, which are within the physiological range in human blood vessels.[28] The experiments were conducted with a 1-h rotation period for evaluation of bacterial and neutrophil adhesion and 4 h for monocyte adhesion.

Bacterial adhesion

A clinical isolate of a *S. epidermidis* bacterial strain RP62A (ATCC 35984) was cultured in tryptic soy broth (Becton Dickinson) overnight at 37°C in an orbital shaker. Subsequent to washing and resuspension in PBS, the bacterial concentration was quantified in colony-forming units per milliliter (cfu/mL) using an optical density measurement at 550 nm by an automated microplate reader (Biotek Instruments). The bacteria was injected at a concentration of 10^8 cfu/mL into a test suspension of either PBS or 25% pooled human serum in the RDS at the start of rotation. Upon rotation for a 60-min time period, a fluid transfer method was used to remove excess nonadherent bacteria from the test suspension. The adherent bacteria were fixed on the polymer surface with 2.5% glutaraldehyde overnight and prepared with serial ethanol drying for scanning electron microscopy (SEM) analysis. The samples were sputter coated and analyzed with SEM for bacterial density measurements at individual shear stress levels.

TABLE I
Phospholipid Polymer Surfaces

Material	Base	Copolymer	Methylene Chain Length
PET	—	—	—
PMB30	PET	Poly(MAPC-*co*-BMA)	2
PMHB30	PET	Poly(MAPC-*co*-BMA)	6